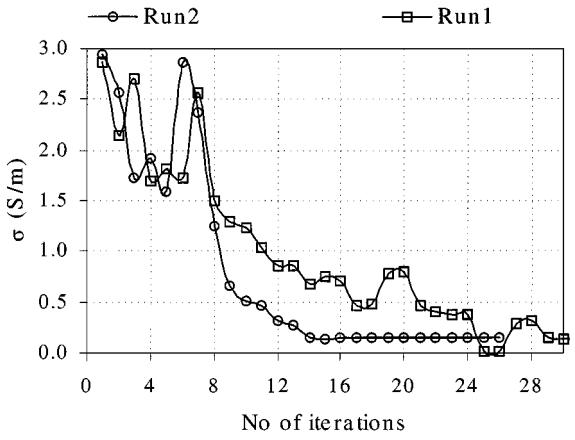

Fig. 4. Convergence of the simulation processes for two different runs for conductivity σ.

Several runs were made and the results of the convergence of two runs are shown in Figs. 3 and 4. After the convergence is reached, the simulated curve for S_{21} matched exactly with the experimental one of Fig. 1, and the permittivity of the sample is reproduced with an accuracy of 0.01%.

IV. Conclusion

Based upon the FEM and a cavity resonance technique, an iterative method for exact estimation of complex permittivity of an arbitrary shaped dielectric has been presented. The measurements are done in a frequency band around any resonance peak, preferably the fundamental one. This paper also defined a number of error parameters used in the process of optimization. The technique can be implemented very easily on a desktop computer for a quick estimation of permittivity of samples on the production line.

Acknowledgment

The authors wish to thank Prof. A. G. Williamson, University of Auckland, New Zealand, and Dr. K. L. Chan, Industrial Research Ltd., Auckland, New Zealand, for critically reading this paper's manuscript.

References

[1] M. N. Afsar, J. R. Birch, and R. N. Clarke, "The measurement of the properties of materials," *Proc IEEE*, vol. 74, pp. 183–199, MONTH 1986.

[2] W. E. Courtney, "Analysis and evaluation of a method of measuring the complex permittivity and permeability of microwave insulators," *IEEE Trans. Microwave Theory Tech.*, vol. MTT-18, pp. 476–485, MONTH 1970.

[3] R. A. Waldron, "Perturbation theory of resonant cavities," *Proc. Inst. Elect. Eng.*, vol. 107C, pp. 272–274, MONTH 1960.

[4] D. Aregba, J. Gay, and G. Maze-Merceur, "Modeling multiport using a three-dimensional coupled analytical/finite element method application to microwave characterization of material," *IEEE Trans. Microwave Theory Tech.*, vol. 42, pp. 590–4, Apr. 1994.

[5] R. Coccioli, G. Pelosi, and S. Selleri, "Characterization of dielectric materials with the finite-element method," *IEEE Trans. Microwave Theory Tech.*, vol. 47, pp. 1106–1111, July 1999.

[6] B. Meng, J. Booske, and R. Cooper, "Extended cavity perturbation technique to determine the complex permittivity of dielectric materials," *IEEE Trans. Microwave Theory Tech.*, vol. 43, pp. 2633–2636, Dec. 1994.

[7] J. K. Vaid, A. Prakash, and A. Mansingh, "Measurement of dielectric parameters at microwave frequencies by cavity perturbation technique," *IEEE Trans. Microwave Theory Tech.*, vol. MTT-27, pp. 791–795, Sept. 1979.

[8] J. M. Jim, *The Finite Element Method in Electromagnetics*. New York: Wiley, 1993.

[9] R. Miniowitz and J. P. Webb, "Analysis of 3-D microwave resonators using covariant-projections elements," *IEEE Trans. Microwave Theory Tech.*, vol. 39, pp. 1895–1899, Nov. 1991.

[10] D. A. H. Jacobs, "A generalization of the conjugate gradient method to solve complex systems," *IMA J. Numer. Anal.*, vol. 6, pp. 447–452, 1986.

A Full-Wave Modal Analysis of Inhomogeneous Waveguide Discontinuities with Both Planar and Circular Cylindrical Boundaries

Robert H. MacPhie and Ke-Li Wu

***Abstract*—A full-wave analysis of an inhomogeneous waveguide region with both planar and circular cylindrical boundaries is presented in this paper. Circular cylindrical modal functions are used to represent the fields. Field matching on the planar walls and apertures is rigorously achieved by the finite plane-wave series expansion of each modal field, whereas the addition theorem for cylindrical waves is used for rigorous field matching on the circular cylindrical boundaries. Numerical results are given for rectangular waveguides with 90° bends and rounded outer corners.**

***Index Terms*—Full-wave modal analysis, inhomogeneous waveguide functions.**

I. Introduction

In a recent paper [1], MacPhie and Wu provided a full-wave modal analysis of waveguide discontinuities with piecewise planar boundaries. Practical examples of such discontinuities are T-, Y-junctions and E- and H-plane mitered 90° bends. In this paper, this technique is extended to discontinuities with both planar and circular cylindrical boundaries. Such an inhomogeneous waveguide discontinuity is shown in Fig. 1, where there are two feeding waveguides, four planar sidewalls, and two circular cylindrical sidewalls. As in [1], the height of the region is w with bottom and top walls at $z = 0$ and $z = w$, respectively.

Bessel–Fourier modal functions are used to represent the TM- (e) and TE-type (h) fields in the inhomogeneous region [1], [2]. For field matching in the planar waveguide apertures A_n and on the planar sidewalls W_m, the finite plane-wave series expansion [1] is employed. However, on the circular cylindrical walls C_l, a rigorous solution is obtained by means of the translation addition theorem [3] for circular cylindrical wave functions. The proposed formula is verified by the comparison of the numerical results obtained by the finite-element method (FEM) and those of the proposed modal analysis for WR75 waveguide 90° bends (both H- and E-planes) having rounded outer corners.

Manuscript received April 26, 2000.

R. H. MacPhie is with the Department of Electrical and Computer Engineering, University of Waterloo, Waterloo, ON N2L 3G1, Canada.

K.-L. Wu is with the Department of Electronic Engineering, The Chinese University of Hong Kong, Shatin, Hong Kong.

Publisher Item Identifier S 0018-9480(01)03981-3.

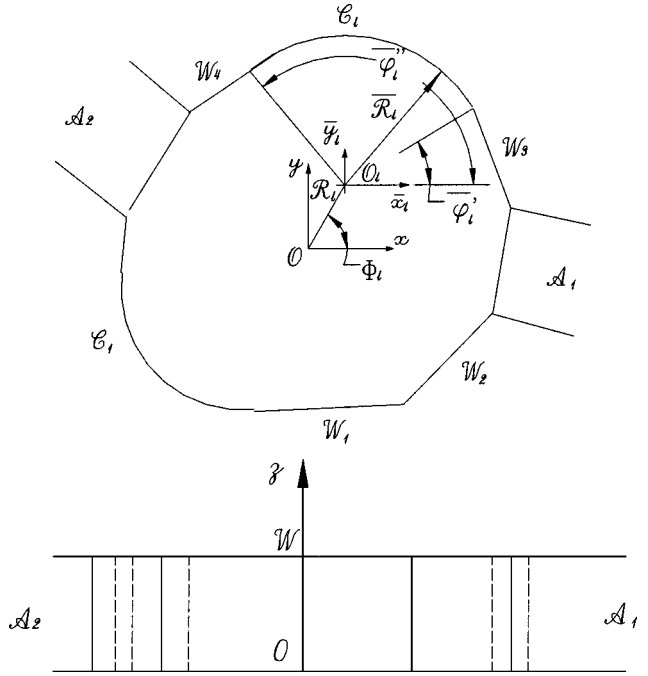

Fig. 1. Inhomogeneous waveguide discontinuity with planar and circular cylindrical boundaries (top and side views).

II. Bessel–Fourier Modal Functions for Inhomogeneous Waveguide Regions with Circular Cylindrical Sectional Boundaries

With reference to Fig. 1, the modal fields in the inhomogeneous region can be obtained from the scalar potentials

$$\Psi^{(e)}_{np\binom{c}{s}}(\rho,\phi,z) = J_n(k_p\rho)\begin{Bmatrix}\cos(n\phi)\\ \sin(n\phi)\end{Bmatrix}\cos\left(\frac{p\pi}{w}z\right) \tag{1}$$

and

$$\Psi^{(h)}_{np\binom{c}{s}}(\rho,\phi,z) = J_n(k_p\rho)\begin{Bmatrix}\cos(n\phi)\\ \sin(n\phi)\end{Bmatrix}\sin\left(\frac{p\pi}{w}z\right) \tag{2}$$

where the origin O of the circular cylindrical system is located centrally in the inhomogeneous region.

We now consider the lth circular cylindrical boundary. The center of the lth circular cylindrical boundary is O_l. R_l is the distance between O and O_l and the angle Φ_l is measured from the x-axis. The boundary extends from $\bar{\phi}_l'$ to $\bar{\phi}_l''$ in the local coordinates $(\bar{\rho}_l, \bar{\phi}_l)$ or $(\bar{x}_l, \bar{y}_l)$ of the lth circular cylindrical boundary C_l. The radius of C_l is $\bar{R}_l$, as shown in the figure for $l = 2$. In Cartesian coordinates, the two ends of the circular boundary C_l are at

$$\begin{aligned}\bar{x}_l' &= \bar{R}_l\cos\bar{\phi}_l' \\ \bar{y}_l' &= \bar{R}_l\sin\bar{\phi}' \end{aligned} \tag{3a}$$

$$\begin{aligned}\bar{x}_l'' &= \bar{R}_l\cos\bar{\phi}_l'' \\ \bar{y}_l'' &= \bar{R}_l\sin\bar{\phi}''. \end{aligned} \tag{3b}$$

Moreover, in terms of the original coordinates (x, y), the two end points of C_l are at

$$\begin{aligned} x_l' &= R_l\cos\phi_l + \bar{x}_l' = R_l\cos\phi_l + \bar{R}_l\cos\bar{\phi}_l' \\ y_l' &= R_l\sin\phi_l + \bar{y}_l' = R_l\sin\phi_l + \bar{R}_l\sin\bar{\phi}_l' \\ x_l'' &= R_l\cos\phi_l + \bar{x}_l'' = R_l\cos\phi_l + \bar{R}_l\cos\bar{\phi}_l'' \\ y_l'' &= R_l\sin\phi_l + \bar{y}_l'' = R_l\sin\phi_l + \bar{R}_l\sin\bar{\phi}_l''. \end{aligned} \tag{4}$$

A. Translation Addition Theorem

We can express $\Psi^{(e)}_{np\binom{c}{s}}(\rho,\phi,z)$ and $\Psi^{(h)}_{np\binom{c}{s}}(\rho,\phi,z)$ in terms of the coordinates of C_l, i.e., $(\bar{\rho}_l, \bar{\phi}_l, \bar{z}_l)$ with $\bar{z}_l = z$ (no axial translation). From Stratton [3, pp. 372–374], we can show that

$$J_n(k_p\rho)\begin{Bmatrix}\cos(n\phi)\\ \sin(n\phi)\end{Bmatrix} = \sum_{q=-\infty}^{\infty} J_{q-n}(k_pR_l)(-1)^{q-n}J_q(k_p\bar{\rho}_l) \bullet \begin{Bmatrix}\cos\left[q\bar{\phi}_l - \bar{\Phi}_{qnl}\right]\\ \sin\left[q\bar{\phi}_l - \bar{\Phi}_{qnl}\right]\end{Bmatrix} \tag{5}$$

where

$$\bar{\Phi}_{qnl} = (q-n)\Phi_l. \tag{6}$$

B. Vector Modal Fields

The modal H-field of TM type is given by

$$\vec{h}^{(e)}_{np\binom{c}{s}}\left(\bar{\rho}_l,\bar{\phi}_l,\bar{z}_l\right) = \nabla\times\hat{z}\Psi^{(e)}_{np\binom{c}{s}}\left(\bar{\rho}_l,\bar{\phi}_l,\bar{z}_l\right) \tag{7}$$

Using (1) and (5) in (7), we can show that

$$\begin{aligned}\vec{h}^{(e)}_{np\binom{c}{s}}\left(\bar{\rho}_l,\bar{\phi}_l,\bar{z}_l\right) = \sum_{q=-\infty}^{\infty} J_{q-n}(k_pR_l)(-1)^{q-n}\cos\left(\frac{p\pi}{w}\hat{z}_l\right) \\ \bullet\left\{q\frac{J_q(k_p\bar{\rho}_l)}{\bar{\rho}_l}\begin{Bmatrix}-\sin\left[q\bar{\phi}_l-\bar{\Phi}_{qnl}\right]\\ \cos\left[q\bar{\phi}_l-\bar{\Phi}_{qnl}\right]\end{Bmatrix}\hat{\rho}_l \right. \\ \left. -k_pJ_q'(k_p\bar{\rho}_l)\begin{Bmatrix}\cos\left[q\bar{\phi}_l-\bar{\Phi}_{qnl}\right]\\ \sin\left[q\bar{\phi}_l-\bar{\Phi}_{qnl}\right]\end{Bmatrix}\hat{\phi}_l\right\}.\end{aligned} \tag{8}$$

From Maxwell's equations, we can then obtain the associated E-field

$$\begin{aligned}&\vec{e}^{(e)}_{np\binom{c}{s}}(\bar{\rho}_l,\bar{\phi}_l,\bar{z}_l) \\ &= \frac{1}{j\omega\varepsilon_0}\sum_{q=-\infty}^{\infty} J_{q-n}(k_pR_l)(-1)^{q-n} \\ &\quad\times\left\{\frac{p\pi}{\omega}\sin\left(\frac{p\pi}{w}\bar{z}_l\right)\bullet\left\{-k_pJ_q'(k_p\bar{\rho}_l)\begin{Bmatrix}\cos\left[q\bar{\phi}_l-\bar{\Phi}_{qnl}\right]\\ \sin\left[q\bar{\phi}_l-\bar{\Phi}_{qnl}\right]\end{Bmatrix}\hat{\rho}_l\right.\right. \\ &\qquad\left.\bullet\begin{Bmatrix}-\sin\left[q\bar{\phi}_l-\bar{\Phi}_{qnl}\right]\\ \cos\left[q\bar{\phi}_l-\bar{\Phi}_{qnl}\right]\end{Bmatrix}\hat{\phi}_l\right\} \\ &\qquad\left.+k_p^2J_q(k_p\bar{\rho}_l)\begin{Bmatrix}\cos\left[q\bar{\phi}_l-\bar{\Phi}_{qnl}\right]\\ \sin\left[q\bar{\phi}_l-\bar{\Phi}_{qnl}\right]\end{Bmatrix}\cos\left(\frac{p\pi}{w}\bar{z}_l\right)\hat{z}_l\right\}.\end{aligned} \tag{9}$$

The modal E-field of TE type is given by

$$\vec{e}^{(h)}_{np\binom{c}{s}}\left(\bar{\rho}_l,\bar{\phi}_l,\bar{z}_l\right) = -\nabla\times\hat{z}\Psi^{(h)}_{np\binom{c}{s}}\left(\bar{\rho}_l,\bar{\phi}_l,\bar{z}_l\right). \tag{10}$$

We can use (2) and (5) in (10) to obtain

$$\begin{aligned}\vec{e}^{(h)}_{np\binom{c}{s}}(\bar{\rho}_l,\bar{\phi}_l,\bar{z}_l) = -\sum_{q=-\infty}^{\infty} J_{q-n}(k_pR_l)(-1)^{q-n}\sin\left(\frac{p\pi}{w}\bar{z}_l\right) \\ \bullet\left\{q\frac{J_q(k_p\bar{\rho}_l)}{\bar{\rho}_l}\begin{Bmatrix}-\sin\left[q\bar{\phi}_l-\bar{\Phi}_{qnl}\right]\\ \cos\left[q\bar{\phi}_l-\bar{\Phi}_{qnl}\right]\end{Bmatrix}\hat{\rho}_l \right. \\ \left. -k_pJ_q'(k_p\bar{\rho}_l)\begin{Bmatrix}\cos\left[q\bar{\phi}_l-\bar{\Phi}_{qnl}\right]\\ \sin\left[q\bar{\phi}_l-\bar{\Phi}_{qnl}\right]\end{Bmatrix}\hat{\phi}_l\right\}.\end{aligned} \tag{11}$$

Again, use of Maxwell's curl equation gives

$$\vec{h}^{(h)}_{np\binom{c}{s}}(\bar{\rho}_l,\bar{\phi}_l,\bar{z}_l) = \frac{1}{j\omega\mu_0}\sum_{q=-\infty}^{\infty} J_{q-n}(k_pR_l)(-1)^{q-n} \times\left\{\left(\frac{p\pi}{w}\right)\cos\left(\frac{p\pi}{w}\bar{z}_l\right) \bullet\left\{k_pJ_q'(k_p\bar{\rho}_l)\left\{\begin{matrix}\cos\left[q\bar{\phi}_l-\bar{\Phi}_{qnl}\right]\\ \sin\left[q\bar{\phi}_l-\bar{\Phi}_{qnl}\right]\end{matrix}\right\}\hat{\rho}_l - q\frac{J_q(k_p\bar{\rho}_l)}{\bar{\rho}_l}\left\{\begin{matrix}\sin\left[q\bar{\phi}_l-\bar{\Phi}_{qnl}\right]\\ -\cos\left[q\bar{\phi}_l-\bar{\Phi}_{qnl}\right]\end{matrix}\right\}\hat{\phi}_l\right\} + k_p^2J_q(k_p\bar{\rho}_l)\left\{\begin{matrix}\cos\left[q\bar{\phi}_l-\bar{\Phi}_{qnl}\right]\\ \sin\left[q\bar{\phi}_l-\bar{\Phi}_{qnl}\right]\end{matrix}\right\}\sin\left(\frac{p\pi}{w}\bar{z}_l\right)\hat{z}_l\right\}. \quad (12)$$

III. Field Matching on the Circular Cylindrical Boundary

The total E-field in the inhomogeneous region is the weighted sum of the e-type and h-type modal fields introduced in Section II as follows:

$$\bar{E}(\bar{\rho}_l,\bar{\phi}_l,\bar{z}_l) = \sum_{np}\left(\alpha^{(e)}_{cnp}\vec{e}^{(e)}_{cnpl} + \alpha^{(e)}_{snp}\vec{e}^{(e)}_{snpl}\right) + \sum_{np}\left(\alpha^{(h)}_{cnp}\vec{e}^{(h)}_{cnpl} + \alpha^{(h)}_{snp}\vec{e}^{(h)}_{snpl}\right). \quad (13)$$

On the lth circular cylindrical boundary C_l, we require that the tangential E-field vanish. Using the modal series (13), we obtain

$$\sum_{np}\left(\alpha^{(e)}_{cnp}\vec{e}^{(e)}_{cnpl,t} + \alpha^{(e)}_{snp}\vec{e}^{(e)}_{snpl,t}\right)+\sum_{np}\left(\alpha^{(h)}_{cnp}\vec{e}^{(h)}_{cnpl,t} + \alpha^{(h)}_{snp}\vec{e}^{(h)}_{snpl,t}\right) = 0 \quad (14)$$

where t indicates the tangential component where $\bar{\rho}_l = \bar{R}_l$ and $\bar{\phi}_l' < \bar{\phi}_l > \bar{\phi}_l''$, as indicated in Fig. 1.

If we take the outer product (cross product) of (14) with $\vec{h}^{(e)}_{c\bar{n}\bar{p}l}$ and $\vec{h}^{(h)}_{c\bar{n}\bar{p}l}$ then, after integration over the surface C_l, we obtain the two linear equations

$$\sum_{np}\left(C^{(ee)}_{\bar{n}\bar{p},np,l}\alpha^{(e)}_{cnp} + Q^{(ee)}_{\bar{n}\bar{p},np,l}\alpha^{(e)}_{snp} + C^{(eh)}_{\bar{n}\bar{p},np,l}\alpha^{(h)}_{cnp} + Q^{(eh)}_{\bar{n}\bar{p},np,l}\alpha^{(e)}_{snp}\right) = 0 \quad (15)$$

and

$$\sum_{np}\left(K^{(ee)}_{\bar{n}\bar{p},np,l}\alpha^{(e)}_{cnp} + S^{(ee)}_{\bar{n}\bar{p},np,l}\alpha^{(e)}_{snp} + K^{(eh)}_{\bar{n}\bar{p},np,l}\alpha^{(h)}_{cnp} + S^{(eh)}_{\bar{n}\bar{p},np,l}\alpha^{(e)}_{snp}\right) = 0. \quad (16)$$

In (15) and (16), if $i = h$ or e and $j = h$ or e, then

$$\begin{bmatrix} C^{(ji)}_{\bar{n}\bar{p},np,l} & K^{(ji)}_{\bar{n}\bar{p},np,l}\\ Q^{(ji)}_{\bar{n}\bar{p},np,l} & S^{(ji)}_{\bar{n}\bar{p},np,l}\end{bmatrix} = \int_0^w\int_{\bar{\phi}_l'}^{\bar{\phi}_l''}\vec{e}^{(i)}_{(\frac{c}{s})npl}\left(\bar{R}_l,\bar{\phi}_l,\bar{z}_l\right) \times\vec{h}^{(i)}_{(\frac{c}{s})\bar{n}\bar{p}l}\left(\bar{R}_l,\bar{\phi}_l,\bar{z}_l\right)\cdot\hat{z}\bar{R}_l d\bar{\phi}_l d\bar{z}_l. \quad (17)$$

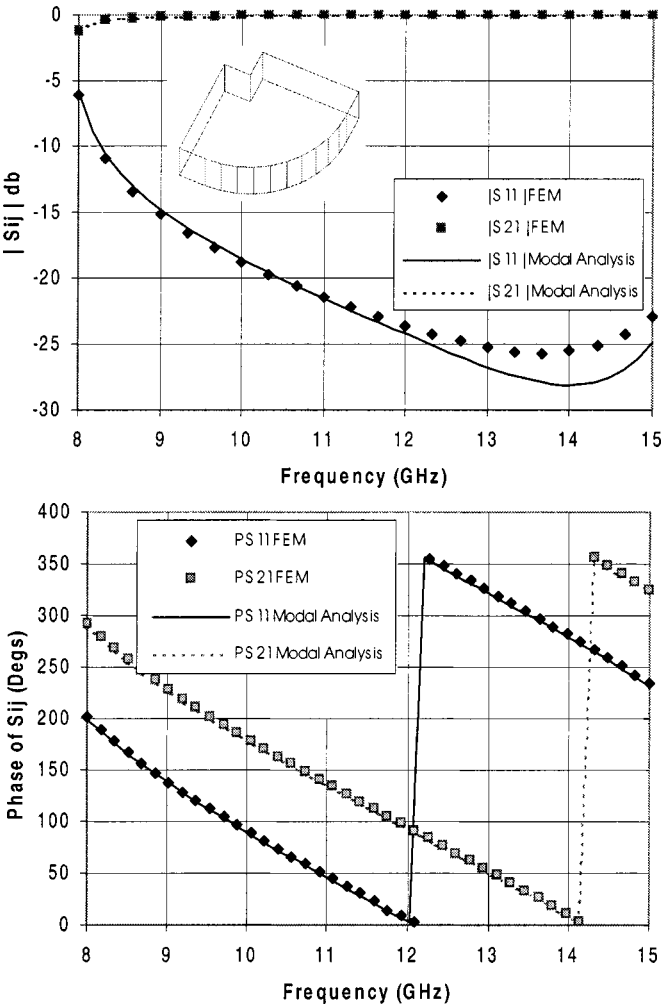

Fig. 2. Magnitude and phase of scattering parameters for a WR75 H-plane curved bend with $\text{radius} = 0.75$ in. The results denoted by dots are calculated by Ansoft's finite-element software HFSS and the results denoted by lines are calculated by the proposed modal analysis.

Likewise, if we take the outer product of (14) with $\vec{h}^{(h)}_{c\bar{n}\bar{p}l}$ and then with $\vec{h}^{(h)}_{s\bar{n}\bar{p}l}$ we obtain, after integration over C_l

$$\sum_{np}\left(C^{(he)}_{\bar{n}\bar{p},np,l}\alpha^{(e)}_{cnp} + Q^{(he)}_{\bar{n}\bar{p},np,l}\alpha^{(e)}_{snp} + C^{(hh)}_{\bar{n}\bar{p},np,l}\alpha^{(h)}_{cnp} + Q^{(hh)}_{\bar{n}\bar{p},np,l}\alpha^{(e)}_{snp}\right) = 0 \quad (18)$$

and

$$\sum_{np}\left(K^{(he)}_{\bar{n}\bar{p},np,l}\alpha^{(e)}_{cnp} + S^{(he)}_{\bar{n}\bar{p},np,l}\alpha^{(e)}_{snp} + K^{(hh)}_{\bar{n}\bar{p},np,l}\alpha^{(h)}_{cnp} + S^{(hh)}_{\bar{n}\bar{p},np,l}\alpha^{(e)}_{snp}\right) = 0. \quad (19)$$

In matrix notation (15), (16), (18), and (19) can be written as

$$\begin{bmatrix}\begin{bmatrix}C^{(ee)}_l\end{bmatrix} & \begin{bmatrix}Q^{(ee)}_l\end{bmatrix} & \begin{bmatrix}C^{(eh)}_l\end{bmatrix} & \begin{bmatrix}Q^{(eh)}_l\end{bmatrix}\\ \begin{bmatrix}K^{(ee)}_l\end{bmatrix} & \begin{bmatrix}S^{(ee)}_l\end{bmatrix} & \begin{bmatrix}K^{(eh)}_l\end{bmatrix} & \begin{bmatrix}S^{(eh)}_l\end{bmatrix}\\ \begin{bmatrix}C^{(he)}_l\end{bmatrix} & \begin{bmatrix}Q^{(he)}_l\end{bmatrix} & \begin{bmatrix}C^{(hh)}_l\end{bmatrix} & \begin{bmatrix}Q^{(hh)}_l\end{bmatrix}\\ \begin{bmatrix}K^{(he)}_l\end{bmatrix} & \begin{bmatrix}S^{(he)}_l\end{bmatrix} & \begin{bmatrix}K^{(hh)}_l\end{bmatrix} & \begin{bmatrix}S^{(hh)}_l\end{bmatrix}\end{bmatrix}\begin{Bmatrix}\alpha^{(e)}_c\\ \alpha^{(e)}_s\\ \alpha^{(h)}_c\\ \alpha^{(h)}_s\end{Bmatrix} = [R_l]\{\alpha\} = 0. \quad (20)$$

The elements of all the matrices are given in detail in the Appendix.

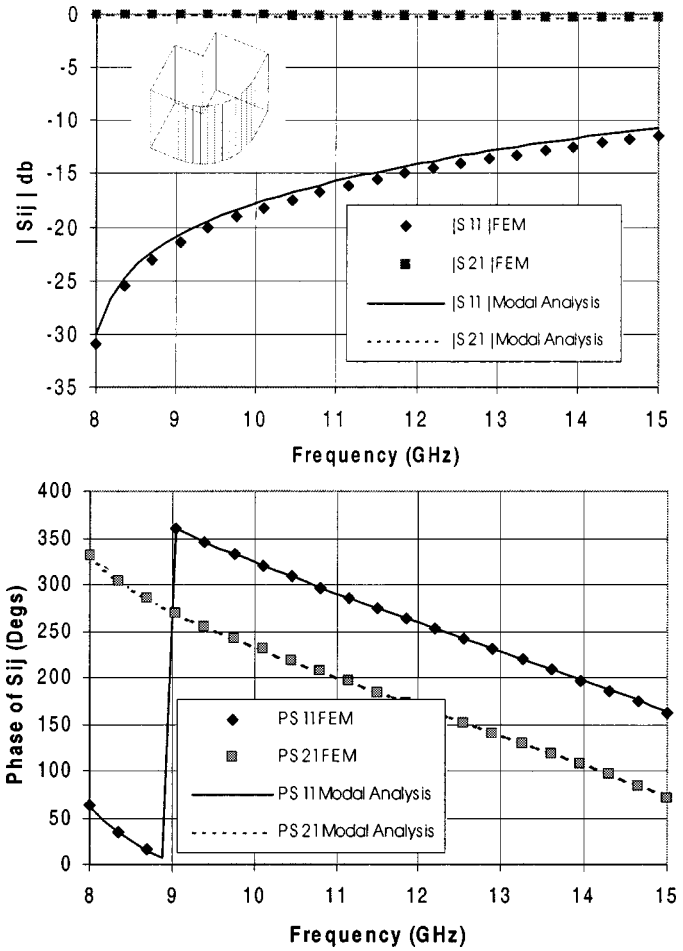

Fig. 3. Magnitude and phase of scattering parameters for a WR75 E-plane curved bend with $\mathrm{radius} = 0.375$ in. The results denoted by dots are calculated by Ansoft's finite-element software HFSS and the results denoted by lines are calculated by the proposed modal analysis.

Having obtained the E-field matching (20) for the lth circular cylindrical boundary of the general inhomogeneous region, we can repeat the process for the remaining circular cylindrical boundaries and let

$$[R] = \sum_{l=1}^{L} [R_l] \tag{21}$$

where L is the total number of circular boundaries. Likewise, for the planar boundaries, we let

$$[W] = \sum_{m=1}^{M} [W_m] \tag{22}$$

where $[W_m]$ is the matrix for the mth planar boundary wall; the elements of $[W_m]$ are given in detail in [1].

The total matrix equation for the conducting wall part of the inhomogeneous region is then

$$\Big([W] + [R]\Big)\{\alpha\} = [T]\{\alpha\} = 0. \tag{23}$$

The field matching in the apertures of the inhomogeneous region is done in the same way as described in [1]. This, in conjunction with (23), leads to the solution for the scattering parameters of the inhomogeneous region, as presented in a detailed fashion in [1].

IV. Numerical Results

The scattering parameters over a wide frequency band for WR75 rectangular waveguide of H- and E-plane 90° bends with rounded outer corners are given in Figs. 2 and 3, respectively. The waveguide dimensions are $a = 0.75$ in and $b = 0.375$ in. With a progressive convergence test, it is found that eight modes for the H-plane bend and six modes for the E-plane bend are sufficient in the inhomogeneous region for a convergent result. Very good agreement between the results of the FEM obtained using Ansoft's HFSS and that of the proposed modal analysis can be observed. The slight discrepancy at high frequencies of the H-plane bend may be contributed by the chamfers at the curved corner in the FEM model. The FEM results are based on the FEM model with about 9000 tetrahedrons.

V. Conclusions

A rigorous modal analysis formula for inhomogeneous waveguide discontinuities containing both planar and circular cylindrical boundaries have been presented in this paper. The addition theorem for Bessel–Fourier functions is used to generalize the formula to handle cylindrical boundaries with arbitrary offset centers. Field matching on the planar walls and apertures of the discontinuous region is rigorously achieved by the finite plane-wave series expansion. Very good agreement is obtained between the results of the FEM and those of the proposed analysis for rectangular waveguide 90° bends with rounded outer corners. Since the generalized scattering matrix (GSM) is obtained by modal analysis, the modules developed by the proposed modal analysis can be easily integrated with other key building blocks of modal analysis for large system design.

Appendix

The elements of the matrices $[C_l^{(ij)}]$, $[Q_l^{(ij)}]$, $[K_l^{(ij)}]$, and $[S_l^{(ij)}]$ for $i = e$ or h and $j = e$ or h are presented here.

In evaluating the outer product integrals, as given by (17), we encounter relatively simple integrals

$$I^l_{1p\bar{p}} = \int_0^w \cos\left(\frac{p\pi}{w}\bar{z}_l\right)\cos\left(\frac{\bar{p}\pi}{w}\bar{z}_l\right)d\bar{z}_l \tag{A1}$$

$$I^l_{2p\bar{p}} = \int_0^w \sin\left(\frac{p\pi}{w}\bar{z}_l\right)\sin\left(\frac{\bar{p}\pi}{w}\bar{z}_l\right)d\bar{z}_l \tag{A2}$$

$$I^l_{1\bar{q}\bar{n},qn} = \int_{\bar{\phi}'_l}^{\bar{\phi}''_l} \cos\left(q\bar{\phi}_l - \bar{\Phi}_{qnl}\right)\cos\left(q\bar{\phi}_l - \bar{\Phi}_{\bar{q}\bar{n}l}\right)d\bar{\phi}_l \tag{A3}$$

$$I^l_{2\bar{q}\bar{n},qn} = \int_{\bar{\phi}'_l}^{\bar{\phi}''_l} \sin\left(q\bar{\phi}_l - \bar{\Phi}_{qnl}\right)\cos\left(q\bar{\phi}_l - \bar{\Phi}_{\bar{q}\bar{n}l}\right)d\bar{\phi}_l \tag{A4}$$

$$I^l_{3\bar{q}\bar{n},qn} = \int_{\bar{\phi}'_l}^{\bar{\phi}''_l} \sin\left(q\bar{\phi}_l - \bar{\Phi}_{qnl}\right)\sin\left(q\bar{\phi}_l - \bar{\Phi}_{\bar{q}\bar{n}l}\right)d\bar{\phi}_l. \tag{A5}$$

We then let

$$\begin{aligned}
\bar{J}^l_{0qnp} &= (-1)^{q-n} J_{q-n}(k_p R_l) J_q\Big(k_p \bar{R}_l\Big) \\
\bar{J}^l_{1qnp} &= (-1)^{q-n} J_{q-n}(k_p R_l) J'_q\Big(k_p \bar{R}_l\Big) \qquad \text{(A6)} \\
\bar{J}^l_{2qnp} &= q\bar{J}^l_{0qnp} \\
\bar{J}^l_{3qnp} &= q\bar{J}^l_{1qnp} \qquad \text{(A7)}
\end{aligned}$$

from which we can define the following double summation:

$$S^l_{ijk,p\bar{n}n} = \sum_{q=-\infty}^{\infty} \sum_{\bar{q}=-\infty}^{\infty} \bar{J}^l_{jqnp} \bar{J}^l_{k\bar{q}\bar{n}p} I^l_{i\bar{q}\bar{n}qn} \tag{A8}$$

where $i = 1, 2, 3$, $j = 0, 1, 2, 3$, and $k = 0, 1, 2, 3$.

With the above definitions, the elements of the 16 submatrices of $[R_l]$, as given by (20), are then as follows, where, due to the orthogonality shown in $I^l_{1,p\bar{p}}$ and $I^l_{2,p\bar{p}}$, by (A1) and (A2), respectively, we can for a given p write

$$C^{(ee)}_{pl,\bar{n}n} = \frac{k_p^2 \bar{R}_l w}{2j\omega\varepsilon_0} S^l_{101,p\bar{n}n}(1+\delta_{p0}) \tag{A9}$$

$$C^{(eh)}_{pl,\bar{n}n} = -\frac{\pi k_p^2 p}{2k_0^2}\left\{S^l_{220,p\bar{n}n}(1+\delta_{p0}) + S^l_{202,p\bar{n}n}(1+\delta_{p0})\right\} \tag{A10}$$

$$C^{(hh)}_{pl,\bar{n}n} = \frac{k_p^3 \bar{R}_l w}{2j\omega\mu_0} S^l_{110,p\bar{n}n}(1+\delta_{p0}) \tag{A11}$$

$$S^{(ee)}_{pl,\bar{n}n} = \frac{k_p^3 \bar{R}_l w}{2j\omega\varepsilon_0} S^l_{301,p\bar{n}n}(1+\delta_{p0}) \tag{A12}$$

$$S^{(eh)}_{pl,\bar{n}n} = -\frac{\pi k_p^2 p}{2k_0^2}\left\{S^l_{221,p\bar{n}n}(1+\delta_{p0}) + S^l_{202,p\bar{n}n}(1+\delta_{p0})\right\} \tag{A13}$$

$$S^{(hh)}_{pl,\bar{n}n} = \frac{k_p^3 \bar{R}_l w}{2j\omega\mu_0} S^l_{310,p\bar{n}n}(1+\delta_{p0}) \tag{A14}$$

$$K^{(ee)}_{pl,\bar{n}n} = \frac{k_p^2 \bar{R}_l w}{2j\omega\varepsilon_0} S^l_{201,p\bar{n}n}(1+\delta_{p0}) \tag{A15}$$

$$K^{(eh)}_{pl,\bar{n}n} = -\frac{\pi k_p^2 p}{2k_0^2}\left\{S^l_{320,p\bar{n}n}(1-\delta_{p0}) - S^l_{102,p\bar{n}n}(1+\delta_{p0})\right\} \tag{A16}$$

$$K^{(hh)}_{pl,\bar{n}n} = \frac{k_p^3 \bar{R}_l w}{2j\omega\mu_0} S^l_{210,p\bar{n}n}(1-\delta_{p0}) \tag{A17}$$

$$Q^{(ee)}_{pl,\bar{n}n} = \frac{k_p^3 \bar{R}_l w}{2j\omega\varepsilon_0} S^l_{201,p\bar{n}n}(1+\delta_{p0}) \tag{A18}$$

$$Q^{(eh)}_{pl,\bar{n}n} = \frac{k_p^2 p}{2k_0^2}\left\{S^l_{131,p\bar{n}n}(1-\delta_{p0}) - S^l_{302,p\bar{n}n}(1+\delta_{p0})\right\} \tag{A19}$$

$$Q^{(hh)}_{pl,\bar{n}n} = \frac{k_p \bar{R}_l w}{2j\omega\mu_0} S^l_{210,p\bar{n}n}(1-\delta_{p0}) \tag{A20}$$

$$C^{(he)}_{pl,\bar{n}n} = S^{(he)}_{pl,\bar{n}n} = K^{(he)}_{pl,\bar{n}n} = Q^{(he)}_{pl,\bar{n}n} = 0. \tag{A21}$$

REFERENCES

[1] R. H. MacPhie and K.-L. Wu, "A full-wave modal analysis of arbitrarily shaped waveguide discontinuities using the finite plane-wave series expansion," *IEEE Trans. Microwave Theory Tech.*, vol. MTT-47, pp. 232–237, Feb. 1999.

[2] J. M. Reiter and F. Arndt, "Rigorous analysis of arbitrarily shaped H- and E-plane discontinuities in rectangular waveguide by a full-wave boundary contour mode-matching method," *IEEE Trans. Microwave Theory Tech.*, vol. 43, pp. 796–801, Apr. 1995.

[3] J. A. Stratton, *Electromagnetic Theory*. New York: McGraw-Hill, 1941.

Analysis of Metallic Waveguides of a Large Class of Cross Sections Using Polynomial Approximation and Superquadric Functions

Sheng-Li Lin, Le-Wei Li, Tat-Soon Yeo, and Mook-Seng Leong

***Abstract*—By using the polynomial approximation and superquadric functions in the Rayleigh–Ritz procedure, a unified method has been proposed to analyze conducting hollow waveguides of a large class of cross sections in our previous paper. Some useful and complicated cross-sectional waveguides in the microwave system, namely, eccentric annular, pentagonal, L-shaped, single-ridged, and double-ridged waveguides are analyzed in this paper. Compared with other numerical methods, this method has the advantages of straightforward, accurate, and computational effective.**

***Index Terms*—Polynomial approximation, Rayleigh–Ritz method, superqaudric functions, waveguide analysis.**

I. INTRODUCTION

The analysis of a uniform metallic hollow waveguide can be carried out by solving the Helmholtz equation and matching boundary conditions on its cross section. A large number of techniques have been proposed in the literature for this purpose: one is the boundary integral–resonant mode expansion (BI-RME) [1]. By using superquadric functions [2], [3] to describe the boundary of the waveguide in the Rayleigh–Ritz method, various cross-sectional waveguides (including rectangular, circular, elliptic, coaxial, triangular, etc.) have been analyzed successfully in a unified manner [4]. In this paper, we extend the application of this method to analyze some waveguides with more complicated cross sections that are commonly used in microwave systems. The cross sections of various hollow metallic waveguides to be analyzed are shown in Fig. 1(a)–(f) for eccentric annular, pentagonal ($N = 4$ and $N = 5$), L-shaped, single-ridged, and double-ridged waveguides.

Analysis of eccentric annular waveguides has been a subject of numerous investigations [5], [6]. In [5], combined with conformal transformation, the method of intermediate problems was used to find the lower bounds and the Rayleigh–Ritz method to find the upper bounds of the cutoff frequency, both for TE and TM modes. A family of new waveguides, pentagonal waveguides [described by *ABCDE* in Figs. 1(b) and 1(c)], has been proposed in [7]. The conformal-mapping finite-difference (CMFD) method was used to analyze its propagation characteristics, and the computed data were compared to some measurement results. L-shaped, single-ridged, and double-ridged waveguides are formed from variations of the rectangular waveguide. They can be used in satellite communication systems for wide-bandwidth operations [8], [9]. The surface integral-equation method (SIE) [10], the finite-element method (FEM) [11]–[13], and the finite-difference method (FDM) [14], [15] have been used to study these structures.

The method in this paper does not need a complex mathematical manipulation (such as conformal mapping) and discretization procedure in the above methods. In Section II, a brief description of the algorithm is given. In Section III, numerical results obtained here are compared with those by other methods and measurement data. A conclusion is drawn in Section IV.

Manuscript received February 10, 2000; revised September 28, 2000. This work was supported by the Ministry of Defense–National University of Singapore Research and Development Commission under Research Grant GR6521.

The authors are with the Department of Electrical and Computer Engineering, National University of Singapore, Singapore 119260 (e-mail: elelilw@nus.edu).

Publisher Item Identifier S 0018-9480(01)03982-5.